

Tropical Indian Ocean response to the decay phase of El Niño in a coupled model and associated changes in south and east-Asian summer monsoon circulation and rainfall

Jasti S. Chowdary¹ · Anant Parekh¹ · Rashmi Kakatkar¹ · C. Gnanaseelan¹ · G. Srinivas¹ · Prem Singh¹ · M. K. Roxy¹

Received: 8 August 2015 / Accepted: 10 October 2015
© Springer-Verlag Berlin Heidelberg 2015

Abstract This study investigates the response of tropical Indian Ocean (TIO) sea surface temperature (SST) to El Niño decay phase and its impacts on South and East Asian summer monsoon in the National Centers for Environmental Prediction Climate Forecast System version 2 free run. The TIO basin-wide warming induced by El Niño at its peak phase (winter; DJF) and next spring (MAM + 1) are reasonably well captured by the model but with weak magnitude. This TIO basin-wide SST warming persists until summer (JJA + 1) and exert strong impact on summer monsoon rainfall and circulation as revealed in the observations. However, TIO SST anomalies are very weak in the model during the El Niño decaying summers. Though El Niño decay is delayed by 2 months in the model, decay of TIO SST warming is faster than the observations. Anomalous latent heat loss from ocean and a feeble southern TIO Rossby waves associated with weak wind response to El Niño are mainly accountable for rapid decay of TIO SST warming by mid-summer in the model. This suggests that JJA + 1 TIO SST response to El Niño decay phase in the model is poorly represented. The model is able to capture the SST anomalies associated with the northwest Pacific anticyclone at the peak phase of El Niño but fail to maintain that during the decay phase in MAM + 1 and JJA + 1. It is found that precipitation and circulation anomalies associated with TIO SST warming over the South and East Asian regions are disorganized in the model during the decay phase of El Niño. Rainfall anomalies over the southwest TIO, west coast of India, northern flank of northwest Pacific anticyclone and over Japan in JJA + 1 are poorly

represented by the model. Analysis of lower troposphere stream function and rotational wind component reveals that northwest Pacific anticyclone shifted far eastward to the date line in the model during JJA + 1 unlike in the observations. Anomalous divergence observed over the western TIO and convergence in the northwest Pacific are absent in the model during JJA + 1. Extension of anomalous tropospheric warming from TIO region to equatorial western Pacific is also very weak in the model due to poor representation of TIO SSTs and the subsequent absence of any Kelvin wave response. Anomalous Walker circulation persisted from DJF to JJA + 1 due to El Niño late decay in the model unlike in the observations. This is also found to be responsible for the redundant changes in SST, rainfall and circulation over the Indo-western Pacific in the model. This study demonstrates that it is essential to represent the decay phase of El Niño and the associated TIO response accurately to have realistic simulations of summer monsoon in the decaying year.

Keywords Indian Ocean warming · Air–sea interactions · Indian summer monsoon · El Niño and southern oscillation (ENSO) · Teleconnections

1 Introduction

Dynamical prediction of seasonal climate depends on the ability to predict slow variations of anomalous boundary forcing such as low frequency variations of sea surface temperature (SST) in tropics (e.g., Charney and Shukla 1981; Palmer and Anderson 1994; Goddard et al. 2001). Global seasonal climate predictability is mostly attributed to teleconnections driven by anomalous convection forced by the tropical Pacific SST anomalies during El

✉ Jasti S. Chowdary
jasti@tropmet.res.in

¹ Indian Institute of Tropical Meteorology, Pune 411008, India

Niño-Southern Oscillation (ENSO; e.g., Brankovic et al. 1994; Stockdale et al. 1998). This important source of low frequency climate variability may be predictable 1 year in advance (e.g., Luo et al. 2008). Further, low frequency SST variations in the tropical Atlantic and Indian Oceans apart from ENSO are the sources of climate anomalies throughout the globe (e.g., Nicholls 1989; Goddard and Graham 1999; Saji and Yamagata 2003; Kushnir et al. 2006).

Tropical Indian Ocean (TIO) climate is strongly influenced by El Niño through atmospheric bridge (e.g., Alexander et al. 2002) and ocean channel (e.g., Sprintall et al. 2014). The first leading mode of the interannual Indian Ocean SST variability is a basin-wide warming or cooling (Yulaeva and Wallace 1994; Klein et al. 1999; Alexander et al. 2002; Chowdary and Gnanaseelan 2007; Yang et al. 2007; Du et al. 2009; Schott et al. 2009; Tao et al. 2014). El Niño induces strong basin-wide SST warming over the TIO in boreal winter (Klein et al. 1999; Alexander et al. 2002). Ocean dynamics in terms of Ekman divergence/convergence and Rossby waves due to changes in surface wind forcing and variations in heat flux associated with El Niño related subsidence plays critical role in inducing TIO basin-wide warming (e.g., Chowdary and Gnanaseelan 2007; Du et al. 2009). This TIO warming, in general, persists for next two seasons until boreal summer (Xie et al. 2009; Chowdary et al. 2011). Whereas warm SST anomalies associated with El Niño in the eastern Pacific weakened or terminated by late boreal spring (e.g., Xie et al. 2010). Persistent TIO warming during the El Niño decaying summer exerts strong impact on South Asian, East Asian and Northwest Pacific monsoon rainfall and circulation (e.g., Wang et al. 2000; Xie et al. 2009; Jiang et al. 2013; Chowdary et al. 2015). During the decay phase of El Niño, Indian summer monsoon (ISM) rainfall is generally normal/above normal (Chowdary et al. 2014), whereas rainfall is below normal over the northwest Pacific (e.g., Xie et al. 2009; Huang et al. 2010), both are highly influenced by TIO warming.

Many of the Coupled Model Intercomparison Project (CMIP) phase 3 and phase 5 (CMIP3 and CMIP5) models, for the Fourth and Fifth Assessment Report (AR4 and AR5; e.g., Meehl et al. 2007; Taylor et al. 2011), capture TIO basin-wide warming well. For example, Du et al. (2013) suggested that half of CMIP5 models capture the key processes responsible for TIO basin-wide warming associated with El Niño. Saji et al. (2006) found that the association between El Niño and TIO basin-wide warming is well resolved in many of the CMIP3 models. Recent study by Tao et al. (2015) demonstrated that in CMIP models oceanic processes offset the weak bias of atmospheric processes in spring, and help to sustain TIO basin-wide warming into summer. They also found that

anomalous northwest Pacific anticyclone is weaker due to weak capacitor effect in many CMIP models. Thus, the ability of Coupled General Circulation Models in capturing the variations of TIO SST in response to El Niño is highly important.

It is clear from aforementioned studies that the variability of South and East Asian summer rainfall and circulation associated with TIO basin-wide warming induced by El Niño is important in the prediction point of view. In the present study, we investigate delayed impact of El Niño on climate over the TIO, ISM and East Asia-Northwest Pacific regions in the coupled general circulation model, the National Centers for Environmental Prediction (NCEP)-Climate Forecasting System version 2 (CFSv2; Saha et al. 2014). Under the National Monsoon Mission of India, CFSv2 is selected as an operational model for dynamical monsoon prediction over the Indian region (<http://www.tropmet.res.in/monsoon/index.php>) and this model has also been widely used for global scale forecast (Saha et al. 2014). It is necessary to evaluate the strengths and weaknesses of the coupled model for regional scale simulation/predictions at inter-annual time scale (e.g., Chowdary et al. 2014). The paper is organized as follows. In Sect. 2, we briefly describe the details of different data and model used in the study. Section 3 demonstrates the TIO response to decay phase of El Niño in the model and provides comparison with the observations. South and East Asian-Northwest Pacific circulation and rainfall during decay phase of El Niño is discussed in Sect. 4. Summary and Discussion are provided in Sect. 5.

2 Model and data used

NCEP-CFSv2 is a coupled model with advanced data assimilation techniques and advanced physics (Saha et al. 2014). The atmospheric component of CFSv2 is Global Forecast System (GFS) with horizontal resolution T126 (~100 km) and 64 sigma layers vertically. The modular ocean model version 4 (MOM4) (Griffies et al. 2004) and a four-layer Noah land-surface model (Ek et al. 2003) are coupled in CFSv2. The CFSv2 model is integrated over a period of 100 years and the last 50 years of model integration are utilized for the analysis. Initial conditions for the atmosphere and the ocean are acquired from NCEP CFS Reanalysis (CFSR; Saha et al. 2010). More details of CFSv2 integrations are provided by Roxy (2014).

The National Oceanic and Atmospheric Administration-National Climatic Data Center (NOAA-NCDC) Extended Reconstructed Sea Surface Temperature (ERSST) version3b (Smith et al. 2008) and Climate Prediction Merged Analysis Precipitation (CMAP; Xie and Arkin 1996) data

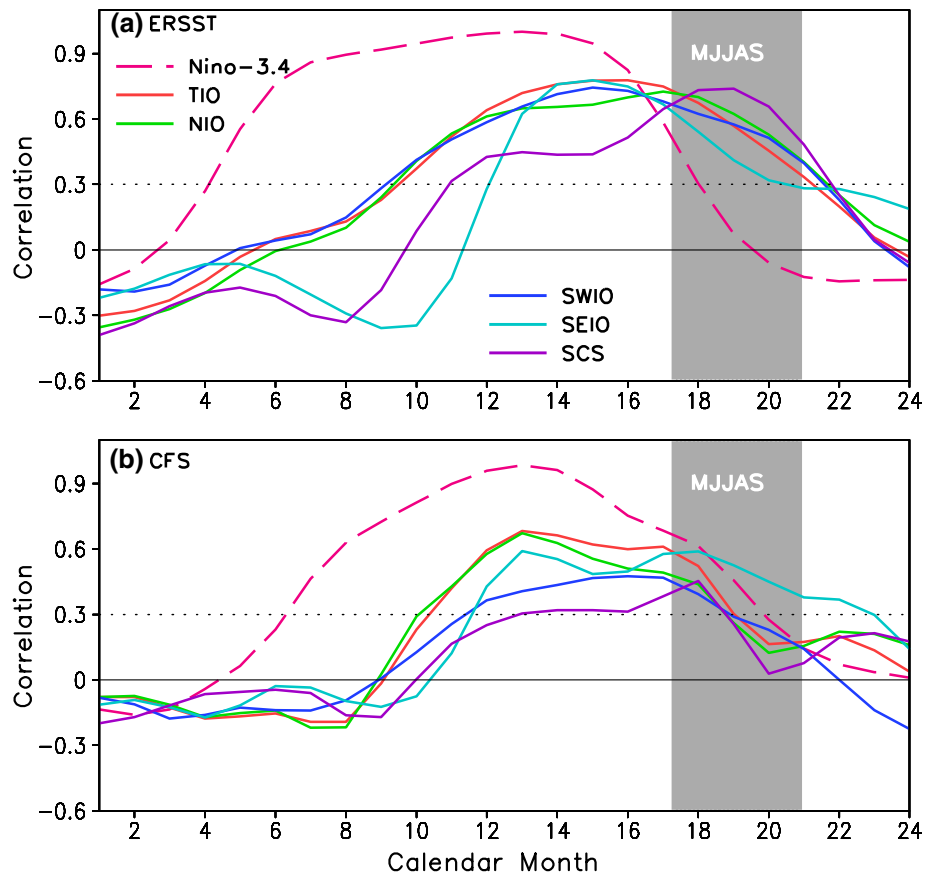
are used for comparison. Observed ocean surface flux components such as short wave radiation (SWR), and latent heat flux (LHF) are obtained from the TropFlux product (Praveen Kumar et al. 2010). Winds (surface, 850 hPa, 200 hPa) and Sea level pressure (SLP) are obtained from European Centre for Medium-Range Weather Forecasts (ECMWF) reanalysis (ERA-Interim; Dee et al. 2011) for the model comparison. In addition to these data sets, ECMWF Ocean reanalysis System (ORA; Balmaseda et al. 2008) sea surface height (SSH) is used for comparison with the model. All observational reanalysis data are based on the period from 1979 to 2013.

Stream function, velocity potential, rotational and divergent component of winds are computed for detailed analysis. Statistical methods such as correlation and regression are used to evaluate the model skill and to understand the physical mechanisms. Results significant at 90 % confidence level based on a two-tailed student's *t* test are discussed. The seasons are defined by those of the northern hemisphere. In the rest of the manuscript DJF (December through February) represents the peak phase of El Niño, spring during decay phase of El Niño is considered as MAM + 1 (March through May), and the following summer is JJA + 1 (June to August).

3 TIO SST response to decay phase of El Niño

Evolution of El Niño cycle during the developing and decay phase is examined in CFSv2 and is compared with the observations. Figure 1 shows the lead lag correlation of DJF Niño-3.4 SST index with the Niño 3.4, TIO, North Indian Ocean (NIO; 50°E to 100°E and equator to 20°N), Southwest tropical Indian Ocean (SWIO; 50°E to 70°E and 15°S to 5°S), Southeast equatorial Indian Ocean (SEIO; 90°E to 110°E and 10°S to equator) and South China Sea (SCS; 105°E to 120°E and 4°N to 20°N) SST. During El Niño developing summers gradual increase in TIO warming is observed from June to September in ERSST (except over the SEIO). It is noted that SCS (SEIO) begins to warm after September (November) in developing years (Fig. 1a). In the model, on the other hand TIO (including SEIO) and SCS display warming only after the summer season (Fig. 1b). Significant warming over the TIO and SCS is seen around August (October) in the model (observations). It is important to note that the El Niño decays before the following summer monsoon in observation, whereas model El Niño decays towards the end of the summer monsoon season displaying about 2 months delay in decay. Prevailing of an excessive equatorial Pacific cold tongue in several

Fig. 1 DJF Niño-3.4 SST index correlation with the TIO (20°S to 20°N and 40°E to 100°E) NIO (Equator to 20°N and 50°E to 100°E), SWIO (15°S to 5°S and 50°E to 70°E), SEIO (10°S to Equator and 90°E to 110°E) and SCS (4°N to 20°N and 105°E to 120°E) SST anomalies during the El Niño developing and decay year **a** ERSST and **b** CFSv2-free run. The dashed thick line (Magenta) is for the lagged autocorrelation of the Niño-3.4 index with DJF SST. Dotted line indicates correlation significant above 90 % confident level



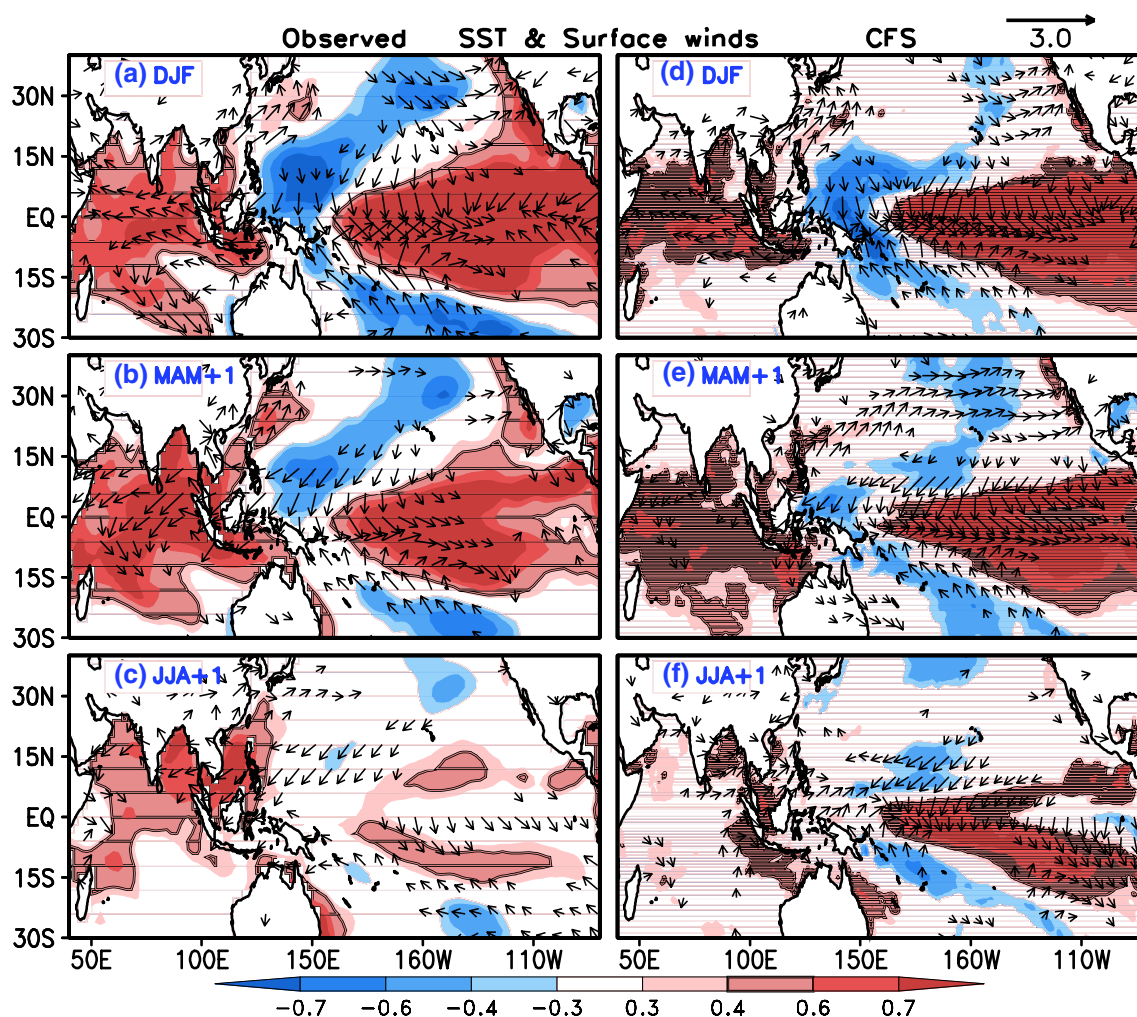


Fig. 2 Correlation of SST (shaded) and surface wind anomalies (vectors) from DJF to JJA + 1 during decay phase of El Niño with DJF Niño-3.4 SST index for **a–c** observations and **d–f** CFSv2-free run. Displayed signals are significant at 90 % confident level

generations of climate models (Mechoso et al. 1995; Yu and Mechoso 1999; Li and Xie 2012, 2014; Zheng et al. 2012) resultants for strengthened SST-thermocline feedback (Li et al. 2015b) and which may be responsible for such an El Niño late decay. SST evolution over the TIO and SCS associated with El Niño is different from observations. Persistent warming observed over the TIO and SCS during summer following peak phase of El Niño (JJA + 1) is not well captured by the model. Model failed to capture the observed lag between Niño 3.4 and TIO SST warming during the decay phase of El Niño.

The characteristics of SST and surface wind anomalies over the Indo-Pacific region during winter (DJF; peak phase of El Niño), spring (MAM + 1) and summer (JJA + 1) are portrayed in Fig. 2. During the peak phase of El Niño zonal extension of near equatorial SST anomalies are well represented in the model when compared to the observations. Convergence of surface winds over central and eastern

Pacific, westerlies east of date line and northwest Pacific anticyclone are also well captured by the model. However, negative SST anomalies over the northwest Pacific, TIO basin-wide warming and equatorial Indian Ocean easterly wind anomalies are weak in the model as compared to the observations (Fig. 2a, d). Spring asymmetric wind pattern over the TIO with northeasterlies in the north of the equator and northwesterlies south of the equator (Wu and Yeh 2010; Chakravorty et al. 2013) and basin-wide warming are weak in the model compared to the observations (Fig. 2b, e) during MAM + 1. Southwesterly wind anomalies in the northern flank of northwest Pacific anticyclone are placed away from the coast in the model unlike in the observations. On the other hand, SST and wind anomaly associated with El Niño over the central and eastern Pacific are well represented by the model in MAM + 1 (Fig. 2b, e). Persistent TIO basin-wide warming, asymmetric wind pattern and northwest Pacific anticyclone are apparent in

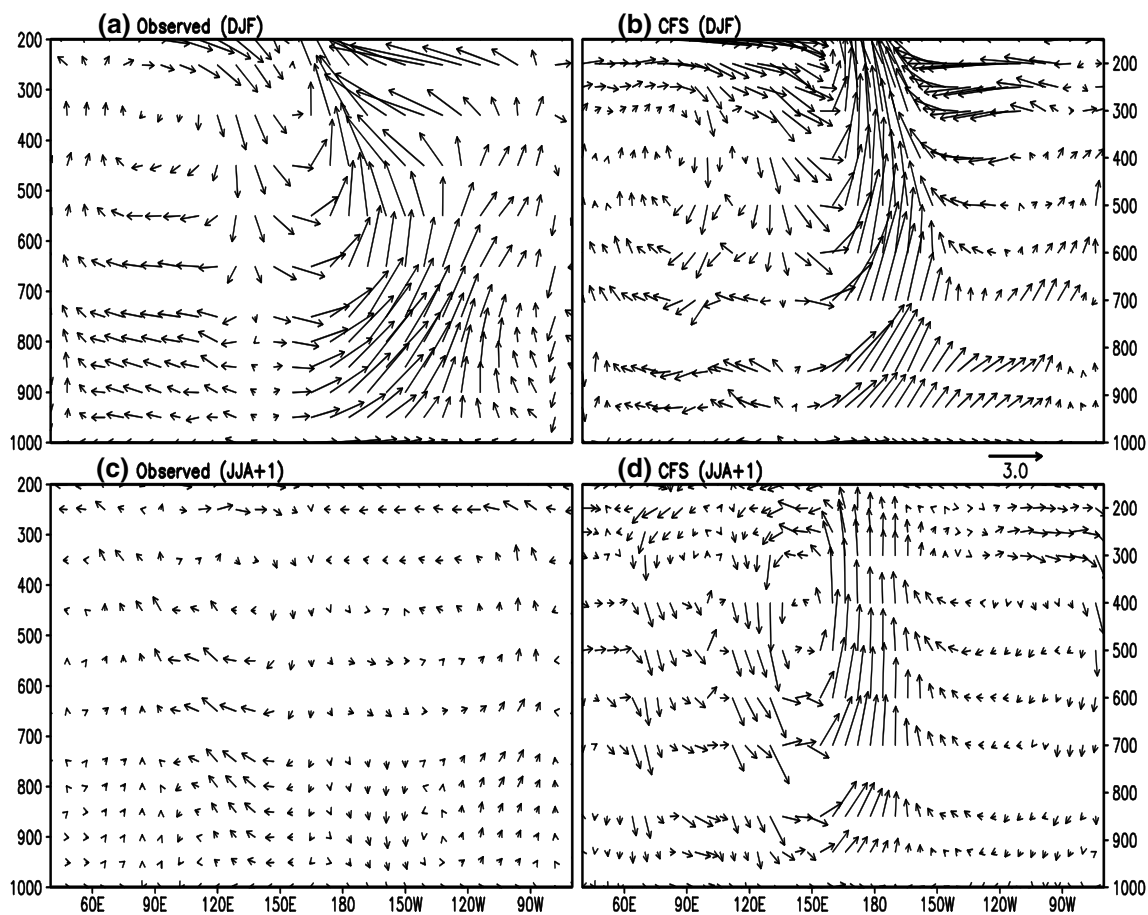


Fig. 3 Regression of zonal and vertical winds (*vectors*, m/s) anomalies averaged (2°S to 2°N) over the equatorial Indian Ocean upon the DJF Niño 3.4 index as a function altitude and longitude for DJF and JJA + 1 for **a**, **c** observations and **b**, **d** CFSv2-free run

observations during JJA + 1 even after El Niño related warming dissipated in the central and eastern Pacific (Fig. 2c). Unlike in the observations, the model displays warm SST anomalies near the date line over the equatorial Pacific region (Fig. 2f). Further, JJA + 1 basin-wide TIO warming and circulation over the northwest Pacific and Indian Ocean regions are not well represented by the model. These results suggest that TIO SST response to El Niño during JJA + 1 is weak in the model. Factors responsible for weak TIO warming during JJA + 1 in the model are further investigated by exploring atmospheric and oceanic processes associated with the decay phase of El Niño.

Changes in the atmospheric circulation over the TIO region due to El Niño induced subsidence through Walker circulation modulates surface heat fluxes and that in turn affects most of the TIO SST (Klein et al. 1999; Venzke et al. 2000; Lau and Nath 2003; Shinoda et al. 2004) in DJF to JJA + 1, except over the southwest TIO. Ascending (descending) branch of Walker circulation associated with El Niño related warm SST anomalies over the equatorial central Pacific (eastern Indian Ocean and western Pacific) is

better represented by the model during DJF as in observations (Fig. 3a, b). Model is also able to capture weak ascending branch over the TIO at peak phase of El Niño. Whereas during JJA + 1, unrealistic descending branch of the Walker circulation is noted in the model over the TIO unlike in the observations (Fig. 3c, d). This subsidence in the model is forced mainly by unrealistic upward motion near the date line due to warm SST anomalies. As a result of this, change in lower tropospheric wind and surface heat flux caused for weak positive SST anomalies over the TIO in the model.

Observations and model show weak negative latent heat flux (negative anomalies represent less heat losing from ocean) as a result of weak winds over most of the TIO in DJF (Fig. 4a, d), which favors SST warming. These latent heat flux anomalies are strong negative over the Bay of Bengal in the model unlike in observations. Shortwave radiation anomalies are positive over the eastern Indian Ocean and western Pacific due to clear sky conditions associated with El Niño induced subsidence, supporting positive SST anomalies (Fig. 2). Over the western and southwestern Indian Ocean, flux components are either weak

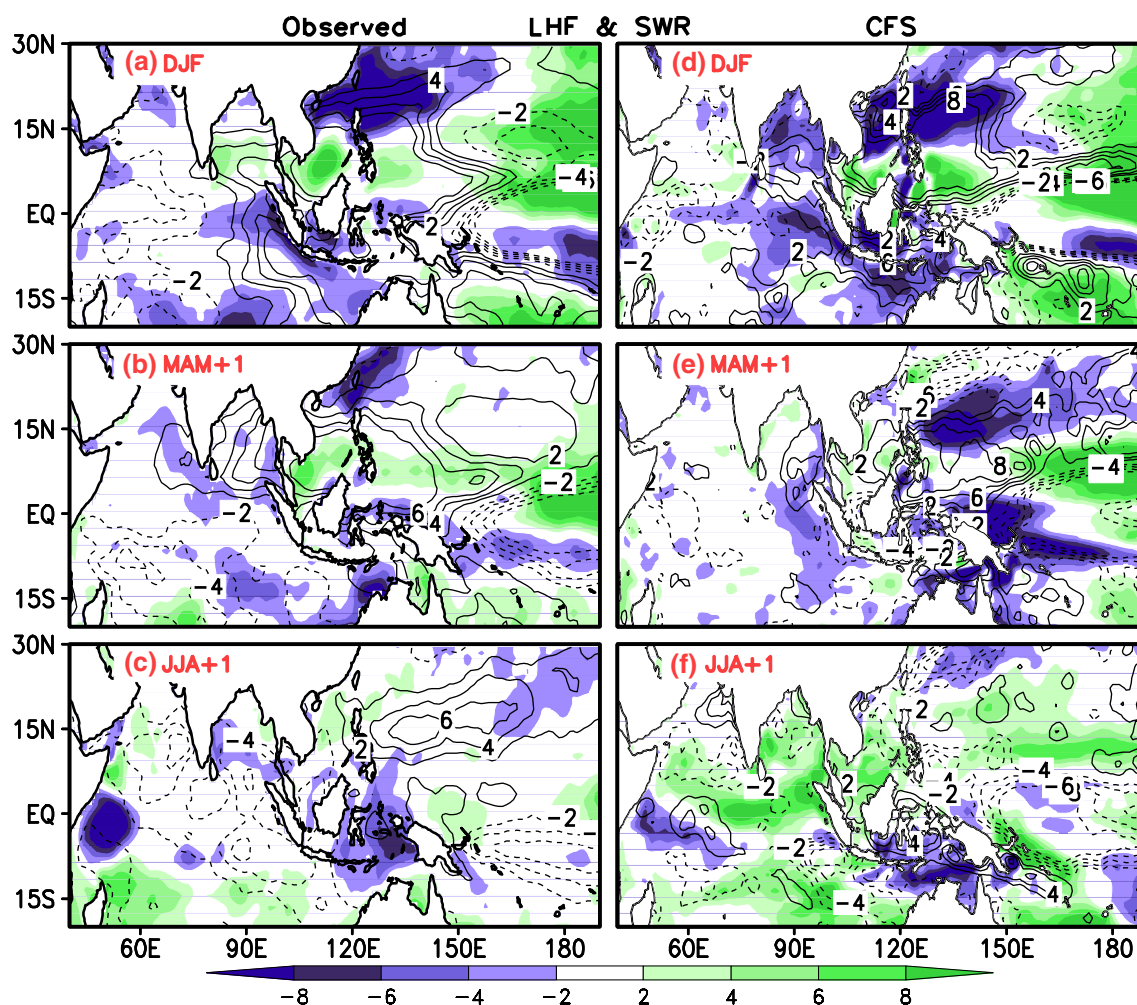


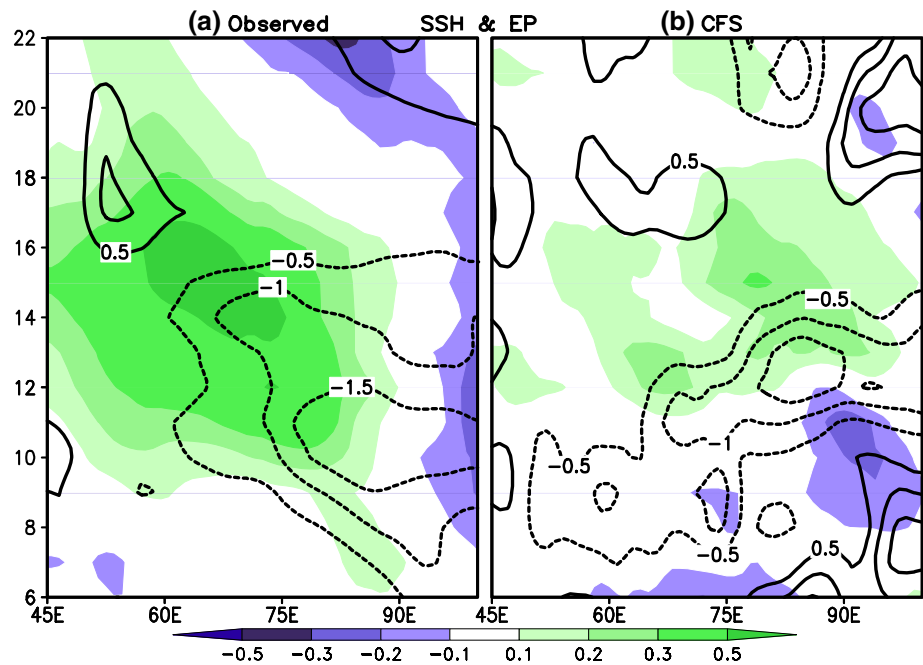
Fig. 4 Regression of Latent heat flux (shaded; Wm^{-2}) and Shortwave radiation (contours; Wm^{-2}) from DJF to JJA + 1 during decay phase of El Niño upon DJF Niño-3.4 SST index for **a–c** observations and **d–f** CFSv2-free run

or out of phase with SST anomalies. This suggests the importance of oceanic processes in maintaining positive SST anomalies especially in MAM + 1 and JJA + 1 in the observations (Fig. 4b, c) and such relationship is weak in the model (Fig. 4e, f). Some discrepancy is noted in representing north–south asymmetry in the short wave radiation anomalies over the TIO and latent heat flux anomaly pattern over northwest Pacific in the model as compared to the observations in MAM + 1. During JJA + 1 surface wind anomalies are against the mean southwesterlies (Fig. 2c), resulting negative latent heat flux anomalies over the NIO (mainly over the Bay of Bengal) as seen in the observations (Fig. 4c). These negative latent flux anomalies help to maintain SST warming over parts of TIO as pointed out by earlier studies (e.g., Du et al. 2009). In case of the model unrealistic strong latent heat flux release to the atmosphere is noted away from the equator (Fig. 4f) and is mainly responsible for trimming down the SST warming over the TIO in JJA + 1. This is mainly due to dry humidity

(negative bias) in the model mean atmosphere (e.g., De et al. 2015). Patterns of both shortwave and latent heat flux are quite unusual over the TIO and northwest Pacific regions in the model. This indicates that persistency of ocean-atmospheric anomalies from MAM + 1 to JJA + 1 over the TIO and northwest Pacific in the model are undermined by warm SST anomalies near the date line through atmospheric adjustments.

As discussed earlier SWIO warming is influenced by ocean dynamics in terms of downwelling Rossby waves (e.g., Xie et al. 2002). Anticyclonic wind stress curl over the south east TIO associated with equatorial easterly wind (stress) anomalies (Fig. 2a, b) in DJF + 1 induced Ekman pumping (Fig. 5a) triggers downwelling Rossby waves (Xie et al. 2002; Gnanaseelan et al. 2008; Chowdary et al. 2009). These westward propagating Rossby waves reach SWIO by JJA + 1 as shown in observed SSH anomalies (Fig. 5a) and help to maintain warming there. Ekman pumping anomalies are short lived and the maximum

Fig. 5 Regression of SSH (shaded, m) and Ekman pumping (contours; 10^{-6} m/s) anomalies averaged over the SIO (from 5°S to 17°S) upon the DJF Niño 3.4 index as a function of calendar month and longitude for **a** observations and **b** CFSv2-free run



values are shifted by a month to December in the model (Fig. 5b). Westward propagating Rossby wave anomalies (as seen in SSH anomalies) are weaker in the model and did not reach the southwest TIO by JJA + 1. The observed coupling between the SSH anomalies and Ekman pumping is not evident in the model. The underestimated SSH anomalies and coupling may be due to a too deep SWIO thermocline dome in model (e.g., Chowdary et al. 2015) as in many other coupled models (e.g., Li et al. 2015a; Zheng et al. 2015). This would largely limit the TIO basin-wide warming response to El Niño. Overall, weak atmospheric anomalies associated with weak ocean response and weak coupling have contributed for the unrealistic TIO SST anomaly pattern over the southern TIO in the model during JJA + 1. Thus TIO response is poor during the decay phase of El Niño and SST anomalies decay faster in model than in the observations.

4 ISM and East Asian-Northwest Pacific circulation and rainfall during the decay phase of El Niño

During the peak phase of El Niño (DJF) positive rainfall anomalies are observed over the western equatorial Indian Ocean, northwestern parts of India and east coast of China along the northern flank of northwest Pacific anticyclone (Fig. 6a). Negative rainfall anomalies over the eastern Indian Ocean and western Pacific are apparent. These spatial distributions of rainfall over the Indo-western Pacific are well captured by the model in DJF (Fig. 6d). Yet the

model displays westward extension of El Niño related rainfall anomalies up to 130°E unlike in the observations. Weare (2012) noted that most of CMIP5 models show westward extension (too far to the west to the western Pacific) of positive precipitation anomalies. Thus this error is common in the coupled models. High SLP and associated circulation at 850 hPa over the Indo-western Pacific region are well represented by the model as compared to the observations (Fig. 6a, d). Reduced strength in the precipitation anomalies over the northwest Pacific is seen in the model during MAM + 1 as in the observations (Fig. 6b, e). Anticyclonic circulation over the northwest Pacific is shifted south and eastward in the model, which is evident in SLP high as well. Circulation anomalies over the TIO are also not well represented in the model in MAM + 1 (Fig. 6e) as observed in Fig. 2. Absence of northeasterly wind anomalies over the Arabian Sea, unrealistic easterly wind anomalies near the maritime continent and eastward shift of northwest Pacific anticyclone (Fig. 6c, f) are the key differences between observations and model in JJA + 1. In addition to that the absence of negative (positive) rainfall anomalies over the northwest Pacific (southwest TIO) and Japan are reported in the model unlike in the observations. These problems in the model arise mainly due to weak response of TIO SST to El Niño decay phase. Apart from El Niño, Indian Ocean Dipole during boreal fall and winter known to modulate subsequent summer monsoon circulation over the northwest Pacific and rainfall (Kripalani et al. 2010).

To further illustrate the Indo-western Pacific circulation response to El Niño (at peak and decay phase), regression

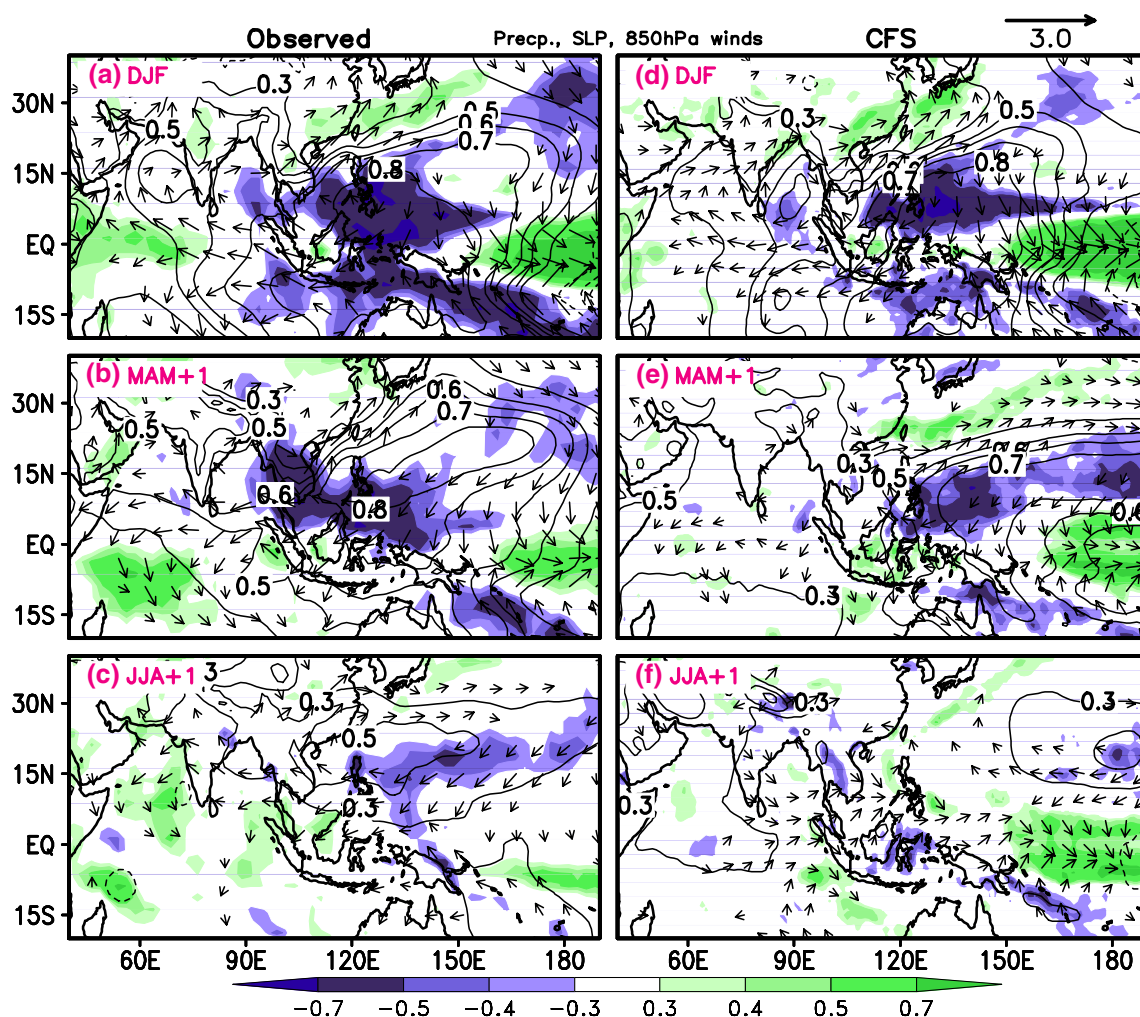


Fig. 6 Correlation of rainfall (shaded), SLP (contours) and 850 hPa wind anomalies (vectors) from DJF to JJA + 1 during decay phase of El Niño with DJF Niño-3.4 SST index for **a–c** observations and **d–f** CFSv2-free run. Displayed signals are significant at 90 % confident level

of DJF Niño 3.4 upon 850 hPa stream function, rotational component of wind (Fig. 7), 200 hPa velocity potential and divergent component of wind (Fig. 8) is presented. As a part of Matsuno (1966), Gill (1980) pattern Rossby wave response to El Niño related SST warming over the equatorial Pacific, two off equatorial cyclonic circulations (on either sides of equator) in the west of date line are apparent in the observations and model (Fig. 7a, d). Symmetric to the equator anomalous anticyclonic circulations over the TIO either sides of the equator are evident in the observation in DJF. These circulation anomalies are weak in the model, indicating poor response of TIO climate to El Niño. Similarly broad 200 hPa convergence zone over the Indo-Western Pacific in response to peak phase of El Niño (200 hPa divergence) is slightly weaker in the model as compared to observations (Fig. 8a, d). By MAM + 1, low level anticyclonic circulation over the southern TIO is weakened and northern hemispheric anticyclone is

shifted to northwest Pacific with core over the Philippines (Fig. 7b). Whereas in the model, intensity of circulation anomalies are weaker than in observations and center of northwestern Pacific anticyclone is shifted towards the east of Philippines (Fig. 7e). Upper level convergence associated with lower level anticyclone over the northwest Pacific is much weaker in the model as compared to observations during MAM + 1 (Fig. 8b, e). In case of JJA + 1 low level northwest Pacific anticyclone in the model has shifted eastward towards the date line unlike in the observations (Fig. 7c, f), leading to suppressed easterly wind anomalies over the NIO region in the model. Further upper level convergence (divergence) over the northwest Pacific (western TIO) is absent in the model (Fig. 8c, f). This analysis suggests that atmospheric response to El Niño is inadequately represented in the model mainly during spring and summer of the decay phase.

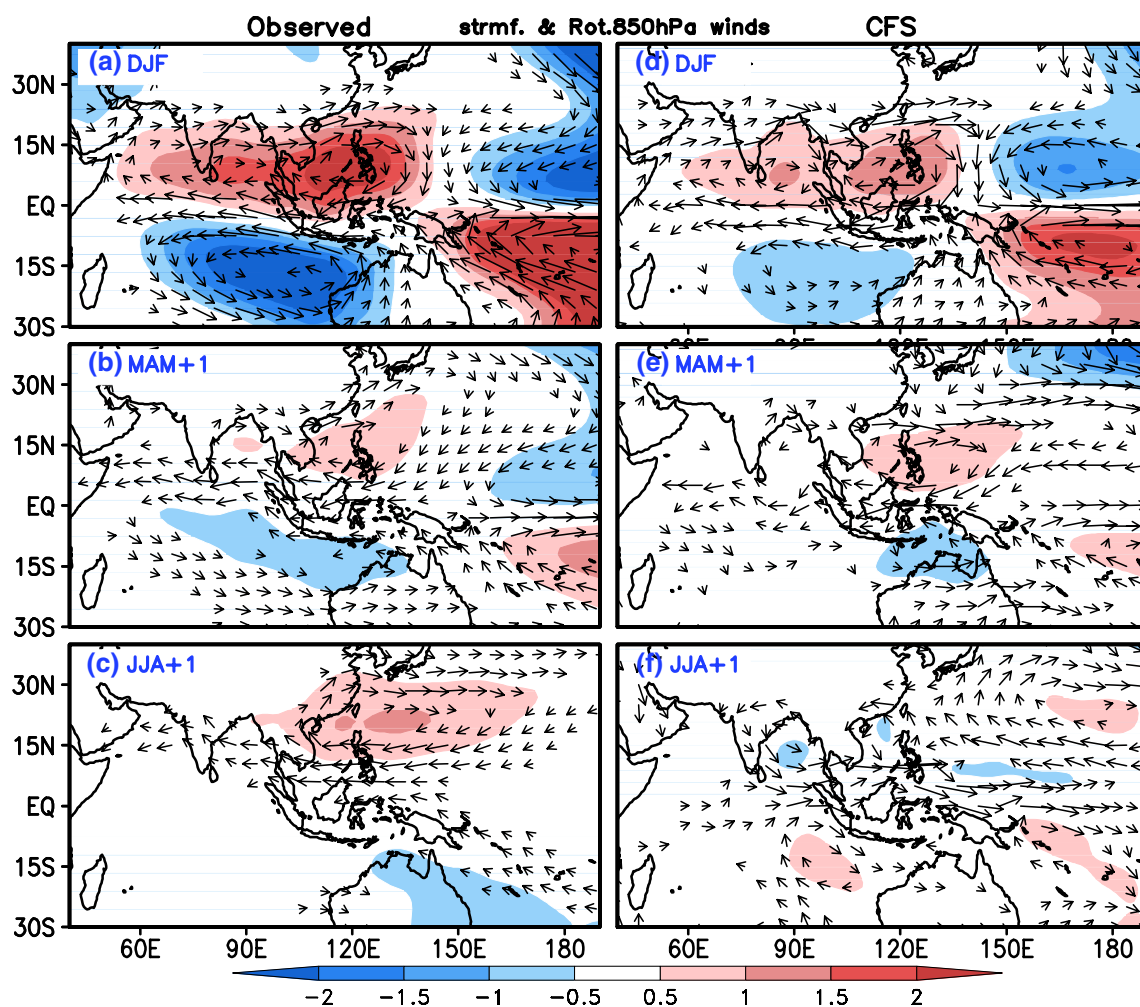


Fig. 7 Regression of 850 hPa Stream function (shaded; $10^6 \text{ m}^3 \text{ s}^{-1}$) and rotational component of wind (vectors; ms^{-1}) from DJF to JJA + 1 during decay phase of El Niño upon DJF Niño-3.4 SST index for **a–c** observations and **d–f** CFSv2-free run

Tropical tropospheric temperature variations are highly related to SST anomalies in the interannual time scale (e.g., Sobel et al. 2002). SST warming associated with El Niño enhances tropospheric temperature warming via deep convection during DJF. Observations show that this warm tropospheric temperature follows Matsuno-Gill type pattern, which is a combined structure of eastward Kelvin and westward off equatorial Rossby waves (Fig. 9a). Most of these features are well captured by the model except over the TIO region (Fig. 9d). As a result of anomalous El Niño conditions, integrated moisture (precipitable water) is maximum over the eastern and central Pacific and minimum over the western Pacific during DJF. Spatial distribution of precipitable water is well represented throughout the tropics during DJF in the model as compared to the observations. El Niño related model tropospheric temperature and precipitable water are weak over the TIO region in MAM + 1 (Fig. 9e). Xie et al. (2009) demonstrated that during JJA + 1 warm tropospheric temperature, in response

to TIO SST warming, propagate into equatorial Pacific and helps to maintain northwest Pacific anticyclone through Kelvin wave-Ekman divergent mechanism. Warm tropospheric temperature and precipitable water with Kelvin wave like pattern over the Indo-western Pacific and strong northwest Pacific anticyclone are apparent during JJA + 1 in the observations (Figs. 9c, 8c, 7c). These signals are not well represented by the model (Figs. 9f, 8f, 7f). Furthermore, eastward Kelvin wave propagation is also evident in the 200 hPa velocity potential anomalies in the observations (Fig. 10a), while the model shows disorganized pattern during JJA + 1 (Fig. 10b). Overall, the Indo-western Pacific climate response during El Niño peak phase or season is fairly well captured by the model, but response is weak in the following spring, which further slide in the summer following El Niño. Representation of TIO SST variation during the decay phase of El Niño in the coupled models is essential for predicting summer monsoon rainfall (e.g., Chowdary et al. 2015).

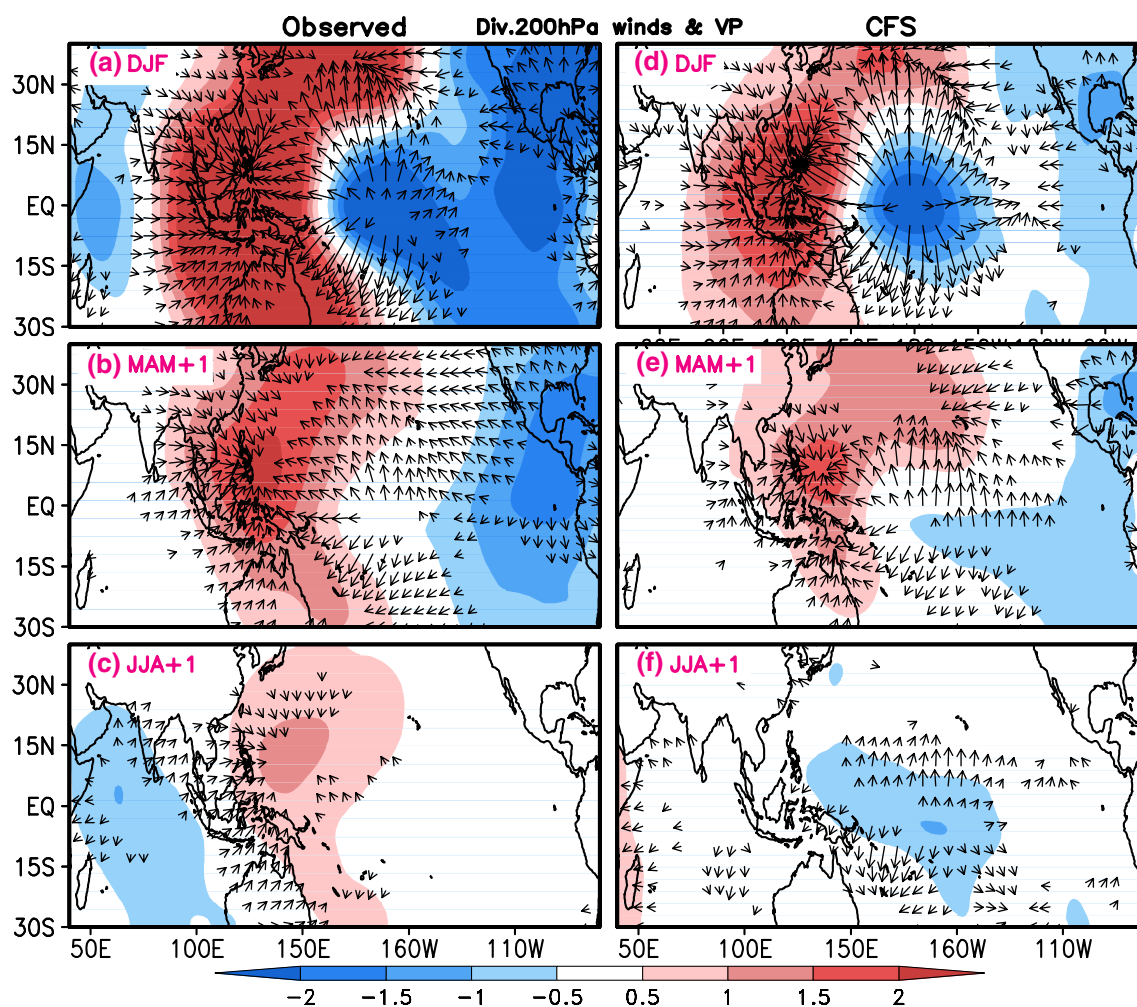


Fig. 8 Regression of 200 hPa Velocity Potential (*shaded*; $10^6 \text{ m}^3 \text{ s}^{-1}$) and divergent component of wind (*vectors*; ms^{-1}) from DJF to JJA + 1 during decay phase of El Niño upon DJF Niño-3.4 SST index for **a–c** observations and **d–f** CFSv2-free run

5 Summary and discussion

Tropical Indian Ocean SST response to El Niño decay phase and changes in rainfall and circulation over the South and East Asian summer monsoon is examined in NCEP-Climate Forecast System version 2 (CFSv2) free run. It is found that in the model (observations) El Niño decay is delayed by 2 months, while TIO warming decays rapidly (slowly) by mid-summer (after summer). During the peak phase of El Niño (winter; DJF) and next spring (MAM + 1) the TIO basin-wide warming is reasonably well captured with weaker magnitude than observed. It is well known that TIO SST warm anomalies persist generally till summer (JJA + 1) and exert strong impact on South and East Asian summer monsoon rainfall and circulation (e.g., Yang et al. 2007; Xie et al. 2009; Chowdary et al. 2015). However, persistent SST warming is very weak in the model during El Niño decay summers. This weak TIO

response to El Niño in MAM + 1 and JJA + 1 is due to anomalous Walker circulation associated with persistent El Niño from DJF to JJA + 1 corresponding to late decay in the model. Anomalous latent heat loss from ocean and feeble southern TIO Rossby waves associated with weak wind response to El Niño have further contributed to the weak TIO SST warming. Over the northwest Pacific the model is able to capture SST anomalies associated with anticyclonic circulation at the peak phase of El Niño but fail to maintain that during the decay phase in MAM + 1 and JJA + 1.

It is noted that positive rainfall anomalies over the southwest TIO and negative rainfall over the South China Sea are weaker than observed in the model during MAM + 1. At the same time rainfall anomalies in the northern flank of northwest Pacific anticyclone observed over the northeast China have shifted towards south in the model. During JJA + 1 anomalous rainfall over the west coast of India and Japan are poorly represented by the model. Poor

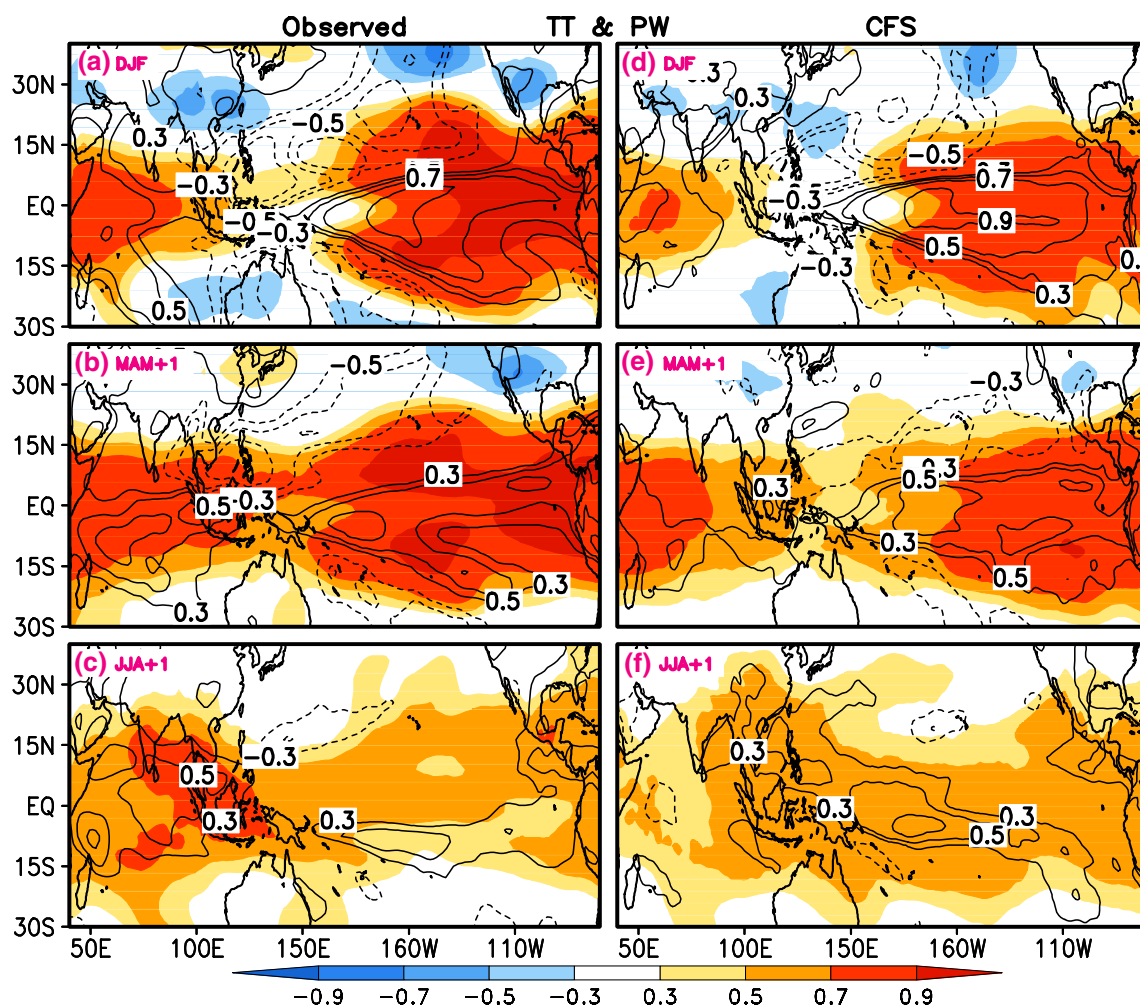


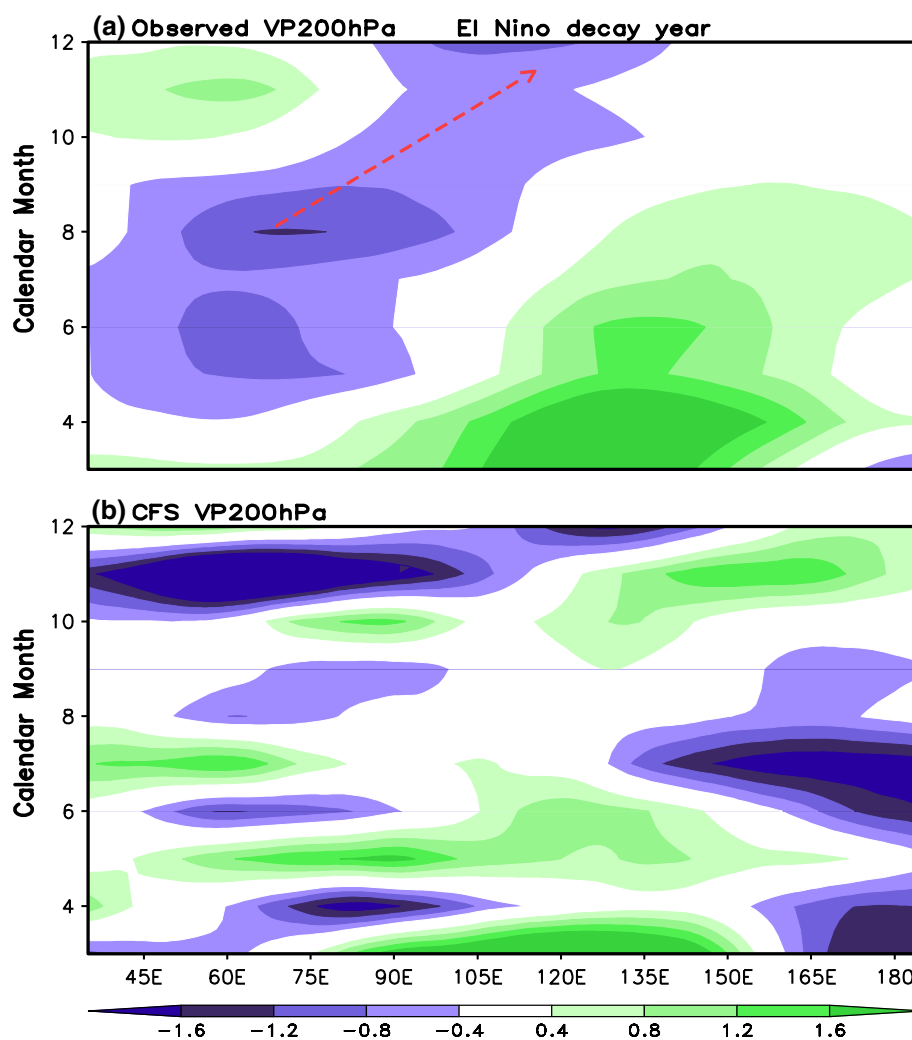
Fig. 9 Correlation of Tropospheric temperature (*shaded*) and Precipitable Water (*contours*) from DJF to JJA + 1 during decay phase of El Niño with DJF Niño-3.4 SST index for **a–c** observations and **d–f** CFSv2-free run

representation of rainfall patterns are in coherence with errors in circulation anomalies. Lower tropospheric stream function and rotational wind component (850 hPa) suggest that cyclonic and anticyclonic circulation over the Indo-western Pacific are well captured by the model during DJF and MAM + 1 but with weaker magnitude. However in JJA + 1 anticyclonic circulation in the southeast TIO weakened and the northwest Pacific anticyclone also shifted far eastward to date line in the model unlike in the observations. This eastward shift of anticyclone apparently is responsible for the absence of easterly/northeasterly wind anomalies over the NIO in the model. Broad upper level convergence (200 hPa) over the eastern Indian Ocean and western Pacific is narrowed down from DJF to MAM + 1 with center over Philippines Sea in the observations. However, this upper level convergence did not persist to JJA + 1 in the model. Overall upper troposphere velocity potential and divergent component of wind anomalies show that anomalous divergence over the western TIO and

convergence over the northwest Pacific are absent in the model during JJA + 1.

El Niño induced tropospheric temperature warming influences the entire tropics by tropical wave dynamics (e.g. Wallace et al. 1998; Sobel et al. 2002). Distribution of this warming is well represented by the model as in observations in most of the tropics except over the eastern TIO and western Pacific during DJF and MAM + 1. Su and Neelin (2002) suggested that this El Niño induced warming pattern in tropics may be modified by the interaction with moist convection. During JJA + 1 TIO warming, in general, supports deep convection and help to enhance the tropospheric temperature as seen in the observations. But such anomalous warming is not apparent in the model. Extension of anomalous tropospheric warming from TIO to equatorial western Pacific as Kelvin wave is also very weak in the model due to poor representation of TIO SSTs. This tropospheric warming in the equatorial western Pacific helps to maintain northwest Pacific anticyclone (Xie et al.

Fig. 10 Regression of 200 hPa Velocity Potential (*shaded* $10^6 \text{m}^3 \text{s}^{-1}$) anomalies averaged (2°S to 2°N) over the equatorial Indian Ocean upon the DJF Niño 3.4 index as a function of calendar month and longitude for **a** observations and **b** CFSv2-free run



2009). Present study advocates that it is essential to capture the decay phase of El Niño and the associated changes in TIO SST accurately in the coupled model. Better representation of TIO SST anomalies in MAM + 1 and JJA + 1 in the model may help to predict rainfall and circulation over the South and East Asian monsoon regions.

Acknowledgments We thank Director IITM for support. We sincerely thank anonymous reviewers for their valuable comments that helped us to improve the manuscript. Figures are prepared using GrADS.

References

- Alexander MA, Blade I, Newman M, Lanzante JR, Lau NC, Scott JD (2002) The atmospheric bridge: the influence of ENSO teleconnections on air–sea interaction over the global oceans. *J Clim* 15(16):2205–2231. doi:[10.1175/1520-0442\(2002\)015<2205:tabtio>2.0.co;2](https://doi.org/10.1175/1520-0442(2002)015<2205:tabtio>2.0.co;2)
- Balmaseda MA, Vidard A, Anderson DLT (2008) The ECMWF ocean analysis system: ORA-S3. *Mon Weather Rev* 136:3018–3034
- Brankovic C, Palmer TN, Ferranti L (1994) Predictability of seasonal atmospheric variations. *J Clim* 7:217–237
- Chakravorty S, Chowdary JS, Gnanaseelan C (2013) Spring asymmetric mode in the tropical Indian Ocean: role of El Niño and IOD. *Clim Dyn* 40:1467–1481. doi:[10.1007/s00382-012-1340-1](https://doi.org/10.1007/s00382-012-1340-1)
- Charney JG, Shukla J (1981) Predictability of monsoons: Monsoon dynamics. In Lighthill J, Sir Pearce RP (eds): Cambridge University Press
- Chowdary JS, Gnanaseelan C (2007) Basin-wide warming of the Indian Ocean during El Niño and Indian Ocean dipole years. *Int J Climatol* 27(11):1421–1438. doi:[10.1002/joc.1482](https://doi.org/10.1002/joc.1482)
- Chowdary JS, Gnanaseelan C, Xie S-P (2009) Westward propagation of barrier layer formation in the 2006–07 Rossby wave event over the tropical southwest Indian Ocean. *Geophys Res Lett* 36:L04607. doi:[10.1029/2008GL036642](https://doi.org/10.1029/2008GL036642)
- Chowdary JS, Xie SP, Luo JJ, Hafner J, Behera S, Masumoto Y, Yamagata T (2011) Predictability of Northwest Pacific climate during summer and the role of the tropical Indian Ocean. *Clim Dyn* 36(3–4):607–621. doi:[10.1007/s00382-009-0686-5](https://doi.org/10.1007/s00382-009-0686-5)
- Chowdary JS, Chaudhari HS, Gnanaseelan C, Parekh A, Rao SA, Sreenivas P, Pokhrel S, Singh P (2014) Summer monsoon circulation and precipitation over the tropical Indian Ocean during ENSO in the NCEP climate forecast system. *Clim Dyn* 42:1925–1947. doi:[10.1007/s00382-013-1826-5](https://doi.org/10.1007/s00382-013-1826-5)

- Chowdary JS, Bandgar AB, Gnanaseelan C, Luo J-J (2015) Role of tropical Indian Ocean air–sea interactions in modulating Indian summer monsoon in a coupled model. *Atmos Sci Lett* 16:170–176. doi:[10.1002/asl2.561](https://doi.org/10.1002/asl2.561)
- De S, Hazra A, Chaudhari HS (2015) Does the modification in “critical relative humidity” of NCEP CFSv2 dictate Indian mean summer monsoon forecast? Evaluation through thermodynamical and dynamical aspects. *Clim Dyn*. doi:[10.1007/s00382-015-2640-z](https://doi.org/10.1007/s00382-015-2640-z)
- Dee DP et al (2011) The ERA-Interim reanalysis: configuration and performance of the data assimilation system. *Q J R Met Soc* 137:553–597
- Du Y, Xie SP, Huang G, Hu K (2009) Role of air–sea interaction in the long persistence of El Niño-induced north Indian Ocean warming. *J Clim* 22(8):2023–2038
- Du Y, Xie S-P, Yang Y-L, Zheng X-T, Liu L, Huang G (2013) Indian Ocean variability in the CMIP5 multimodel ensemble: the basin mode. *J Clim* 26(18):7240–7266. doi:[10.1175/jcli-d-12-00678.1](https://doi.org/10.1175/jcli-d-12-00678.1)
- Ek MB, Mitchell KE, Lin Y, Rogers E, Grunmann P, Koren V, Gayno G, Tarplay JD (2003) Implementation of Noah land surface model advances in the National Centers for environmental prediction operational mesoscale Eta model. *J Geophys Res* 108(D22):8851. doi:[10.1029/2002JD003296](https://doi.org/10.1029/2002JD003296)
- Gill AE (1980) Some simple solutions for heat-induced tropical circulation. *Q J R Meteorol Soc* 106(449):447–462. doi:[10.1256/smsqj.44904](https://doi.org/10.1256/smsqj.44904)
- Gnanaseelan C, Vaid BH, Polito PS (2008) Impact of biannual Rossby waves on the Indian Ocean Dipole. *IEEE Geosci Remote Sens Lett* 5(3):427–429. doi:[10.1109/LGRS.2008.919505](https://doi.org/10.1109/LGRS.2008.919505)
- Goddard L, Graham NE (1999) The importance of the Indian Ocean for simulating rainfall anomalies over eastern and southern Africa. *J Geophys Res* 104:19099–19116
- Goddard L, Mason SJ, Zebiak SE, Ropelewski CF, Basher R, Cane MA (2001) Current approaches to seasonal-to-interannual climate predictions. *Int J Climatol* 21:1111–1152
- Griffies S, Harrison MJ, Pacanowski RC, Anthony R (2004) A Technical Guide to MOM4. GFDL Ocean Group Technical Report No. 5. Princeton NJ: NOAA/Geophysical Fluid Dynamics Laboratory: 342 pp
- Huang G, Hu KM, Xie SP (2010) Strengthening of tropical Indian Ocean teleconnection to the Northwest Pacific since the Mid-1970s: an atmospheric GCM study. *J Clim* 23(19):5294–5304. doi:[10.1175/2010jcli3577.1](https://doi.org/10.1175/2010jcli3577.1)
- Jiang X, Yang S, Li J, Li Y, Hu H, Lian Y (2013) Variability of the Indian Ocean SST and its possible impact on summer western North Pacific anticyclone in the NCEP Climate Forecast System. *Clim Dyn* 41:2199–2212
- Klein SA, Soden BJ, Lau N-C (1999) Remote sea surface temperature variations during ENSO: evidence for a tropical atmospheric bridge. *J Clim* 12(4):917–932
- Kripalani RH, Oh JH, Chaudhari HS (2010) Delayed influence of the Indian Ocean dipole mode on the East Asia–West Pacific monsoon: possible mechanism. *Int J Climatol* 30:197–210
- Kushnir Y, Robinson WA, Chang P, Robertson AW (2006) The physical basis for predicting Atlantic sector seasonal-to-interannual climate variability. *J Clim* 19:5949–5970
- Lau NC, Nath MJ (2003) Atmosphere–ocean variations in the Indo-Pacific sector during ENSO episode. *J Clim* 16:3–20
- Li G, Xie S-P (2012) Origins of tropical-wide SST biases in CMIP multi-model ensembles. *Geophys Res Lett* 39:L22703. doi:[10.1029/2012GL053777](https://doi.org/10.1029/2012GL053777)
- Li G, Xie S-P (2014) Tropical biases in CMIP5 multimodel ensemble: the excessive equatorial Pacific cold tongue and double ITCZ problems. *J Clim* 27:1765–1780
- Li G, Du Y, Xu H, Ren B (2015a) An intermodel approach to identify the source of excessive equatorial Pacific cold tongue in CMIP5 models and uncertainty in observational datasets. *J Clim*. doi:[10.1175/JCLI-D-15-0168.1](https://doi.org/10.1175/JCLI-D-15-0168.1)
- Li G, Xie S-P, Yan D (2015b) Climate model errors over the South Indian Ocean thermocline dome and their effect on the basin mode of interannual variability. *J Clim* 28:3093–3098
- Luo JJ, Mason S, Behera SK, Yamagata T (2008) Extended ENSO prediction using a fully coupled ocean–atmosphere model. *J Clim* 21:84–93
- Matsuno T (1966) Quasi-geostrophic motions in the equatorial area. *J Meteor Soc Japan* 44(1):25–43
- Mechoso CR et al (1995) The seasonal cycle over the tropical Pacific in coupled ocean–atmosphere general circulation models. *Mon Weather Rev* 123:2825–2838
- Meehl GA, Covey C, Taylor KE, Delworth T, Stouffer RJ, Latif M, McAvaney B, Mitchell JFB (2007) THE WCRP CMIP3 multimodel dataset: a new era in climate change research. *Bull Am Meteorol Soc* 88(9):1383–1394. doi:[10.1175/bams-88-9-1383](https://doi.org/10.1175/bams-88-9-1383)
- Nicholls N (1989) Sea surface temperatures and Australian winter rainfall. *J Clim* 2:965–973
- Palmer TN, Anderson DLT (1994) Prospects for seasonal forecasting: a review paper. *Q J R Meteorol Soc* 120:755–793
- Praveen Kumar B, Vialard J, Lengaigne M, Murty VSN, McPhaden MJ (2010) TropFlux: air–sea fluxes for the global tropical oceans—description and evaluation against observations. *Clim Dyn* 38:1521–1543
- Roxy M (2014) Sensitivity of precipitation to sea surface temperature over the tropical summer monsoon region and its quantification. *Clim Dyn* 43:1159–1169. doi:[10.1007/s00382-013-1881-y](https://doi.org/10.1007/s00382-013-1881-y)
- Saha S, Moorthi S, Pan HL, Wu X, Wang J, Nadiga S, Tripp P, Kistler R, Woollen J, Behringer D, Liu H, Stokes D, Grumbin R, Gayno G, Wang J, Hou YT, Chuang HY, Juang HMH, Sela J, Iredell M, Treadon R, Kleist D, Delst PV, Keyser D, Derber J, Ek M, Meng J, Wei H, Yang R, Lord S, van den Dool HM, Kumar A, Wang W, Long C, Chelliah M, Xue Y, Huang B, Higgin W, Zou CZ, Liu Q, Chen Y, Han Y, Cucurull L, Reynolds RW, Rutledge G, Goldberger M (2010) The NCEP climate forecast system reanalysis. *Bull Am Meteorol Soc* 91:1015–1057. doi:[10.1175/2010BAMS3001.1](https://doi.org/10.1175/2010BAMS3001.1)
- Saha S, Moorthi S, Wu X, Wang J, Nadiga S, Tripp P, Pan HL, Behringer D, Hou Y-T, Chuang H-Y, Mark I, Ek M, Meng J, Yang R (2014) The NCEP climate forecast system version 2. *J Clim* 27:2185–2208. doi:[10.1175/JCLI-D-12-00823.1](https://doi.org/10.1175/JCLI-D-12-00823.1)
- Saji NH, Yamagata T (2003) Possible impacts of Indian Ocean dipole mode events on global climate. *Clim Res* 25:51–169
- Saji NH, Xie SP, Yamagata T (2006) Tropical Indian Ocean variability in the IPCC twentieth-century climate simulations. *J Clim* 19(17):4397–4417. doi:[10.1175/jcli3847.1](https://doi.org/10.1175/jcli3847.1)
- Schott FA, Xie SP, McCreary JP (2009) Indian Ocean circulation and climate variability. *Rev Geophys* 47:100. doi:[10.1029/2007rg000245](https://doi.org/10.1029/2007rg000245)
- Shinoda T, Alexander MA, Hendon HH (2004) Remote response of the Indian Ocean to interannual SST variations in the tropical Pacific. *J Clim* 17:362–372
- Smith TM, Reynolds RW, Peterson TC, Lawrimore J (2008) Improvements to NOAA’s historical merged land–ocean surface temperature analysis (1880–2006). *J Clim* 21:2283–2296
- Sobel AH, Held IM, Bretherton CS (2002) The ENSO signal in tropical tropospheric temperature. *J Clim* 15:2702–2706
- Sprintall J, Gordon AL, Lee T, Potemra JT, Pujiana K, Wijffels SE (2014) The Indonesian seas and their role in the couple ocean–climate system. *Nat Geosci* 7:487–492. doi:[10.1038/ngeo2188](https://doi.org/10.1038/ngeo2188)
- Stockdale TN, Anderson DLT, Alves JOS, Balmaseda MA (1998) Global seasonal rainfall forecasts using a coupled ocean–atmosphere model. *Nature* 392:370–373
- Su H, Neelin JD (2002) Teleconnection mechanisms for tropical Pacific descent anomalies during El Niño. *J Atmos Sci* 59:2694–2712

- Tao W, Huang G, Hu K, Qu X, Wen G, Gong Y (2014) Different influences of two types of El Niños on the Indian Ocean SST variations. *Theor Appl Climatol* 117(3–4):475–484. doi:[10.1007/s00704-013-1022-x](https://doi.org/10.1007/s00704-013-1022-x)
- Tao W, Huang G, Hu K, Gong H, Wen G, Liu L (2015) A study of biases in simulation of the Indian Ocean basin mode and its capacitor effect in CMIP3/CMIP5 models. *Clim Dyn*. doi:[10.1007/s00382-015-2579-0](https://doi.org/10.1007/s00382-015-2579-0)
- Taylor KE, Stouffer RJ, Meehl GA (2011) An overview of CMIP5 and the experiment design. *Bull Am Meteorol Soc* 93(4):485–498. doi:[10.1175/bams-d-11-00094.1](https://doi.org/10.1175/bams-d-11-00094.1)
- Venzke S, Latif M, Villwock A (2000) The coupled GCMECHO-2. Part II: Indian Ocean response to ENSO. *J Clim* 13:1371–1383
- Wallace JM, Rasmusson EM, Mitchell TP, Kousky VE, Sarachik ES, von Storch H (1998) On the structure and evolution of ENSO-related climate variability in the tropical Pacific: Lessons from TOGA. *J Geophys Res* 103(C7):14,241–14,259
- Wang B, Wu R, Fu X (2000) Pacific-east Asian teleconnection: how does ENSO affect east Asian climate. *J Clim* 13:1517–1536
- Weare BC (2012) El Niño teleconnections in CMIP5 models. *Clim Dyn*. doi:[10.1007/s00382-012-1537-3](https://doi.org/10.1007/s00382-012-1537-3)
- Wu R, Yeh SW (2010) A further study of the tropical Indian Ocean asymmetric mode in boreal spring. *J Geophys Res* 115:D08101. doi:[10.1029/2009JD012999](https://doi.org/10.1029/2009JD012999)
- Xie P, Arkin PA (1996) Analyses of global monthly precipitation using gauge observations, satellite estimates and numerical model predictions. *J Clim* 9:840–858
- Xie SP, Annamalai H, Schott FA, McCreary JP (2002) Structure and mechanisms of south Indian Ocean climate variability. *J Clim* 15(8):864–878
- Xie SP, Hu K, Hafner J, Tokinaga H, Du Y, Huang G, Sampe T (2009) Indian Ocean capacitor effect on Indo-western Pacific climate during the summer following El Niño. *J Clim* 22(3):730–747
- Xie SP, Du Y, Huang G, Zheng XT, Tokinaga H, Hu KM, Liu QY (2010) Decadal shift in El Niño influences on Indo-Western Pacific and East Asian climate in the 1970s. *J Clim* 23(12):3352–3368. doi:[10.1175/2010jcli3429.1](https://doi.org/10.1175/2010jcli3429.1)
- Yang J, Liu Q, Xie S, Liu Z, Wu L (2007) Impact of the Indian Ocean SST basin mode on the Asian summer monsoon. *Geophys Res Lett* 34(2):L02708. doi:[10.1029/2006gl028571](https://doi.org/10.1029/2006gl028571)
- Yu J-Y, Mechoso CR (1999) Links between annual variations of Peruvian stratocumulus clouds and of SST in the eastern equatorial Pacific. *J Clim* 12:3305–3318
- Yulaeva E, Wallace JM (1994) Signature of enso in global temperature and precipitation fields derived from the microwave sounding unit. *J Clim* 7(11):1719–1736. doi:[10.1175/1520-0442\(1994\)007<1719:tso eig>2.0.co;2](https://doi.org/10.1175/1520-0442(1994)007<1719:tso eig>2.0.co;2)
- Zheng Y, Lin JL, Shinoda T (2012) The equatorial Pacific cold tongue simulated by IPCC AR4 coupled GCMs: upper ocean heat budget and feedback analysis. *J Geophys Res*. doi:[10.1029/2011JC007746](https://doi.org/10.1029/2011JC007746)
- Zheng X-T, Gao L, Li G, Du Y (2015) The southwest Indian Ocean thermocline dome in CMIP5 models: historical simulation and future projection. *Adv Atmos Sci*. doi:[10.1007/s00376-015-5076-9](https://doi.org/10.1007/s00376-015-5076-9)